DISEASE IN WILDLIFE OR EXOTIC SPECIES

Intrasarcoplasmic Polyglucosan Inclusions in Heart and Skeletal Muscles of Long-Finned Pilot Whales (*Globicephala melas*) May be Age-Related

Camille M Longué[*], Mark P Dagleish[†], Gillian McGovern[‡], Andrew C Brownlow[§] and Johanna L Baily[†,‖]

[*]Royal (Dick) School of Veterinary Studies, University of Edinburgh, Easter Bush, [†]Moredun Research Institute, Pentlands Science Park, Penicuik, [‡]Animal and Plant Health Agency, Pentlands Science Park, Penicuik, [§]Scottish Marine Animal Stranding Scheme, SRUC Northern Faculty, Inverness Campus, Inverness and [‖]Institute of Aquaculture, University of Stirling, Stirling, Scotland, UK

Correspondence to: M P Dagleish (e-mail: mark.dagleish@moredun.ac.uk)

Accepted refereed manuscript of: Longué C, Dagleish M, McGovern G, Brownlow A & Baily J (2020) Intrasarcoplasmic Polyglucosan Inclusions in Heart and Skeletal Muscles of Long-Finned Pilot Whales (Globicephala melas) may be Age-Related. *Journal of Comparative Pathology*, 181, pp. 18-25. https://doi.org/10.1016/j.jcpa.2020.09.011

Summary

Polysaccharide storage myopathies have been described in several animal species and are characterised by periodic Acid–Schiff (PAS)-positive, diastase-resistant intrasarcoplasmic inclusions in myocytes. Skeletal and cardiac muscle samples from a subset of a single pod of stranded long-finned pilot whales (*Globicephala melas*) were evaluated by light and transmission electron microscopy. Twelve individuals demonstrated sporadic basophilic packets of PAS-positive, diastase-resistant complex polysaccharide material, either centrally or peripherally in skeletal and cardiac myocytes. Few microscopic myopathic changes were found but included focal inflammation and internalized nuclei. Ultrastructurally, the inclusions consisted of loosely arranged, tangled filaments and were not membrane-bound, which is consistent with polyglucosan bodies. Within skeletal muscle, the number of inclusions had a marginal statistically significant ($p = 0.0536$) correlation with length, as a proxy for age, suggesting that such inclusions in skeletal muscles may be age-related, although the cause remains unclear.

Introduction

Polyglucosan bodies are periodic-Acid–Schiff (PAS)-positive and diastase-resistant intracytoplasmic inclusions composed of poorly branched, long strands of abnormal glycogen with a characteristic fibrillar ultrastructure (Cheville, 2009). In humans, they occur as incidental, age-related changes, such as in corpora amylacea in neural tissue or basophilic degeneration of the myocardium, and also as pathological accumulations as a key feature of the wide ranging polyglucosan body diseases (Cavanaugh, 1999). They occasionally occur in skeletal or cardiac muscle in conditions such as Lafora body disease, or as a primary lesion sites of myopathies, including glycogen-storage disorders types IV, VII and XV, and AMP-activated protein kinase deficiency (Cavanaugh, 1999; Hedberg-Oldfors and Oldfors, 2015). In animals, polyglucosan body accumulation in muscle has been most thoroughly characterized in equine polysaccharide storage myopathy (EPSM) (Valentine *et al*, 1997).

Specific carbohydrate metabolism pathway dysfunctions have been identified for most of these disorders, including Type 1 EPSM (Hedberg-Oldfors and Oldfors, 2015; McCue *et al*, 2008). Clinical signs referable to muscle, vary with disease subtype in people, but generally include muscle weakness and atrophy, and exercise intolerance (Hedberg-Oldfors and Oldfors, 2015). Similarly, clinical signs in EPSM depend on chronicity, with muscle fasciculations and stiffness observed in the acute presentation and muscle atrophy and gait abnormalities in the chronic form (Valberg *et al*, 2011).

Similar intramyofibre PAS-positive, diastase-resistant aggregates and granules have been described within the skeletal muscles of 11 cetacean species, including short-finned pilot whales (*Globicephala macrorhynchus*) (Sierra *et al*, 2012) and within the myocardium of pilot whales (Scotti, 1962; Cowan, 1966). Inclusions in skeletal muscle were accompanied by chronic myopathic changes, muscle atrophy and necrosis (Sierra *et al*, 2012), whereas those in heart were considered akin to age-related “basophilic degeneration” in humans

(Cowan, 1966). However, the pathogenesis and clinical significance of polyglucosan inclusions in cetaceans remain undetermined.

Long-finned pilot whales (*Globicephala melas*) are large pelagic odontocetes, the Northern and Southern subspecies of which, inhabit boreal and subarctic parts of the Atlantic Ocean and circumpolar Antarctic Ocean, respectively. Pod size is typically 10 to 20 closely related members, thought to be formed around adult females and their offspring (Reeves *et al*, 2002). Pilot whales are commonly involved in both mass and single strandings with 254 strandings of individual animals in Scotland alone in the six-year period of 2005–2019 (Scottish Marine Animal Stranding Scheme, 2020).

This aim of this study was to describe and characterize intrasarcoplasmic inclusions in skeletal and cardiac muscles from 12 long-finned pilot whales from a single pod involved in a mass stranding event (MSE) to determine if they were pathological, age-related or a combination of both.

Materials and Methods

Animals and Samples

Thirty-nine pilot whales from a single pod of approximately 70 animals, presumed to be genetically-related, stranded on July 22, 2011 at the Kyle of Durness, Scotland, UK (58°32'1.2516" N, -4°48'9.252" W) and 19 are known to have died following a re-flotation attempt. Sixteen pilot whales (8 females and 8 males) ranging in length from 2.83–5.55 m were recovered and necropsied on site. Where possible, the age of individual animals (Table 1) was estimated retrospectively on the basis of tooth analysis (Luque *et al*, 2009).

Necropsies were performed according to a standard protocol (Kuiken and Baker, 1991) and a wide range of tissue samples from each animal was collected for histological evaluation.

Skeletal muscle samples were taken from the *longissimus dorsi* muscle immediately

craniolateral to the leading edge of the dorsal fin after the blubber had been removed. Ventricular myocardium was also sampled. Tissues for histology were fixed in 10% neutral buffered formalin, processed routinely through graded alcohols, embedded in paraffin wax, sectioned (4μm) and mounted on glass slides. Initial diagnostic histology on haematoxylin and eosin (HE)-stained sections allowed selection of 12 individuals (seven females and five males) based on histological assessment of post-mortem tissue preservation sufficient to permit sensible interpretation. Serial sections were cut from skeletal and cardiac muscle samples and stained with HE, PAS or PAS-diastase (PAS-D) (Bancroft and Cook, 1994). Additional heart and skeletal muscle serial sections were taken from two representative individuals and stained with Grocott–Gomori's methenamine silver (GGMS), toluidine blue or von Kossa (Bancroft and Cook, 1994) to assess the presence of carbohydrate, acidic residues and mineralization, respectively. All sections were evaluated for the presence or absence of the following changes: cytoplasmic vacuolation, inflammation, small group atrophy, myocyte regeneration, myocyte degeneration, haemorrhage, fibrosis and parasitism.

Quantification and Statistical Analyses

For skeletal muscle only, the numbers of angular fibres and internalized nuclei were counted in 10 random microscopic fields at a final magnification of ×200. The total number of polyglucosan inclusion-containing myocytes was counted in each section stained with HE, PAS or PAS-D. To standardise the inclusion counts across muscle types and sections, the area of each tissue section was measured using AnalySIS (Soft Imaging System software, Olympus, Tokyo, Japan). The inclusion density was calculated by dividing the total inclusion count on the slide by the total area of that tissue section.

To establish a mean cell diameter for each sample, the diameters of two cells devoid of inclusions were measured in PAS-stained sections from each of five random microscopic

fields at ×200 magnification. For every inclusion, the diameter of the inclusion and the diameter of the cell containing it, were measured using AnalySIS. The proportion of the cell occupied by the inclusion was estimated by dividing the area of the inclusion by the area of the host cell, and multiplying by 100, to give a relative percentage. Means were calculated for inclusion diameter, the diameter of cells containing inclusions and the diameter of cells devoid of inclusions.

As the diameter of skeletal muscle cells was highly correlated with the length of the whale ($p < 0.001$), the inclusion density, based on standardized number of myocytes, was used for analysis. This was calculated by multiplying the inclusion density by the average myocyte cross-sectional area from the sample.

Statistical analyses were performed using R software (version 2.15.1, R Foundation for Statistical Computing, Vienna, Austria). Analysis of variance was used to compare categorical variables (sex, muscle type, and presence of inflammation and degeneration) and linear models were used to compare continuous variables (length and density of inclusions, and percentage of cell occupied by inclusions). Approximation to normality was judged by means of the Shapiro-Wilks W test. The results indicate that log(x-1) gave the best transformation. For all analyses, $p \leq 0.05$ was considered significant.

Electron Microscopy

One mm^3 samples of skeletal muscle were taken from 4 pilot whales (SW2011/303.01, SW2011/303.09, SW2011/303.13 and SW2011/303.04) that were suitably well-preserved and had relatively higher numbers of inclusions, as detected by light microscopy, post-fixed in osmium tetroxide, dehydrated and embedded in Epon resin 812 (Hexion, Columbus, Ohio, USA) for electron microscopy. Myocardial tissue was extracted from a paraffin wax block (SW2011/303.01) and prepared for electron microscopy as above.

Sections (1 µm) from all resin-embedded samples were stained with toluidine blue. Intrasarcoplasmic inclusions were identified in the skeletal muscle of whale SW2011/303.09 and myocardium of whale SW2011/303.01. Sections from these two blocks were serially sectioned at 60 nm, stained with uranyl acetate and lead citrate (Ellis, 2007) and examined with a Joel 1200EX transmission electron microscope (Joel, Tokyo, Japan).

Results

Histopathology

Ten of the 12 cases demonstrated minimal (0 to 2 per ×200 field) intrasarcoplasmic inclusions in both cardiac and skeletal muscle samples in HE-, PAS- and PAS-D-stained sections. The remaining two cases (SW2011/303.02, SW2011/303.11) contained only a single intrasarcoplasmic inclusion in either cardiac or skeletal myocytes, which were only observed in PAS- and PAS-D-stained sections.

The cardiac and skeletal muscle inclusions were morphologically identical, had sharply demarcated borders and frequently appeared as discrete or aggregated packets (Fig. 1), although sometimes they appeared as uniform amorphous aggregates. In HE-stained sections, the inclusions varied from pale to deeply basophilic, occasionally with a darker staining centre, and were located both peripherally and centrally within the myocyte sarcoplasm. The myocytes that contained inclusions were frequently perifascicular or on the edge of perimysium and often appeared to displace myofibrils and, in cardiac muscle, also displace nuclei. The inclusions were positive in PAS-stained serial sections, staining bright pink, and were resistant to diastase digestion (Fig. 2), positive for carbohydrate with GGMS (Fig. 3a), metachromatic with toluidine blue, indicative of acidic residues (Fig. 3b) and were devoid of mineralization with von Kossa staining.

In a few sections, small inflammatory foci were centred on inclusion-containing myocytes and composed of macrophages, predominantly, with fewer lymphocytes and neutrophils (Fig. 4a). Some macrophages contained PAS-positive, diastase-resistant material (Fig. 4b). The affected myocytes were degenerate as indicated by loss of cross-striations and a markedly fragmented sarcolemma resulting in a "moth-eaten" appearance. A moderate number of internalised myocyte nuclei were present. None of the samples examined showed vacuolation, small group atrophy, regeneration, haemorrhage, fibrosis, fat infiltration, or protozoal or metazoan parasites.

Electron Microscopy

By electron microscopy, the skeletal muscle myocytes, recognized by light microscopy as containing diastase-resistant inclusions, were seen to contain several large aggregates of non-membrane bound filamentous material in both sarcoplasmic and subsarcolemmal locations (Fig. 5a). This material was frequently interspersed with, and displaced, the myofibrils. The inclusions consisted of irregularly arranged filaments, often with more electron-dense cores in which individual filaments could not be discerned, while other inclusions appeared less well aggregated and were composed of loosely arranged, short, tangled and randomly-oriented filaments (Fig. 5b). Consistently, inclusions which contained an electron-dense core also appeared more compact and electron-dense with fewer visible filaments.

In the cardiac myocytes, inclusions were present in central or peripheral locations and distributed between myofibrils, often displacing them (Fig. 6a). These inclusions were morphologically very similar to those in the skeletal muscle, consisting of moderately electron-dense, short, non-membrane bound filaments that were randomly oriented, loosely amassed and frequently contained a homogeneous more electron-dense core (Fig. 6b). Both inclusion types were deemed consistent with polyglucosan bodies.

Quantitative and Statistical Analyses

The mean densities of inclusions in PAS-stained skeletal and cardiac muscle sections were 2.40/cm^2 and 5.39/cm^2, respectively. In the same sections, where present, the mean proportion of cell occupied by inclusions was 64.1% and 72.5% in skeletal and cardiac muscle, respectively. There was a marginally significant correlation ($p = 0.0536$) between the inclusion density, based on standardized number of myofibres and whale length in muscle samples, based on examination of PAS-stained sections. No correlation was found between the number of inclusions per standardized number of myofibres and whale length in myocardium. There were no correlations between the number of inclusions per standardised number of myofibres with sex or presence of inflammation, degeneration or angular fibres, nor between the percentage of myocyte cell diameter occupied by inclusions with sex or length.

Discussion

The basophilic inclusions documented in this study appear similar to those reported in the skeletal muscles of other cetacean species (Sierra *et al*, 2012). However, we characterized the changes using different parameters, including frequency, density, proportion of cell occupied, and presence in myocardium, which was more appropriate to our goal of determining if the inclusions were age-related rather than disease-related. Furthermore, ultrastructural examination, in addition to the histological and histochemical analyses, revealed that the inclusions were consistent with polyglucosan bodies.

Electron microscopy demonstrated that, like those found in EPSM and human polyglucosan body diseases, the inclusions in this study were not membrane-bound, which suggests they originated intracellularly. Most, but not all, contained more electron dense

206 cores, which could represent progressive consolidation of material (Valentine *et al*, 1997;
207 Cavanaugh, 1999; McCue *et al*, 2009). The displacement of cardiac and skeletal myofibrils
208 was also reported in EPSM, in which it was proposed to play a role in the pathogenesis of
209 muscle dysfunction (Naylor *et al*, 2012). Glycogen accumulation is proposed to be one of the
210 initial steps in the formation of diastase-resistant complex polysaccharide in EPSM
211 (Valentine and Cooper, 2006). Glycogen granules or aggregates were not identified
212 ultrastructurally or histologically in this study, as diastase-sensitive material could have been
213 depleted during the live-stranding process or lost through routine processing of the tissues.
214 The identical staining characteristics and ultrastructure of the inclusions in cardiac
215 and skeletal muscle and simultaneous presence in both tissues in most cases (83%), are
216 suggestive of a shared pathogenesis, likely involving a defect in carbohydrate metabolism. In
217 addition to cardiac and skeletal muscle, polysaccharide inclusions have been found in various
218 smooth muscles of horses with EPSM, including urinary bladder, ureter, penis and arrector
219 pili muscles (Larcher *et al*, 2008). However, there were no inclusions in smooth muscle in the
220 sections examined from the pilot whales in the present study (Brownlow *et al*, 2015). The
221 foci of inflammation, centred on inclusion-containing myocytes, suggests that a pathological
222 process leads to its accumulation, and the presence of a moderate number of internalised
223 nuclei in some skeletal muscle sections is indicative of chronic myopathy. However, there
224 was no associated atrophy or acute necrosis as described in other cetaceans (Sierra *et al*,
225 2012). Ubiquitin, which targets abnormal proteins, has been reported in polysaccharide
226 inclusion-containing myocytes in cetaceans (Sierra *et al*, 2012) and horses (Valentine *et al*,
227 2006), further supporting a pathological origin. Ubiquitination of glycogen aggregates is
228 proposed to play a role in the development of diastase resistance (Valentine and Cooper,
229 2006), potentially in response to abnormal folding of the glycogenin protein component of

glycogen (Valentine *et al*, 2006). Unfortunately, immunolabelling for ubiquitin was not performed in our study due to limited funds.

Although only marginally statistically significant, most likely due to the small sample size of this pod, there was a correlation between the inclusion density by standardized number of myofibres and whale length in skeletal muscle samples. Length being used as a proxy for age, this finding suggests that intrasarcoplasmic polyglucosan inclusions in skeletal muscles may be age-related in this species. This finding is supported by previous reports, in which, with the exception of a single juvenile bottlenose dolphin, polysaccharide inclusions in skeletal muscle of other cetacean species were only found in adult or adult–senile specimens (Sierra *et al*, 2012). Accumulation of PAS-positive inclusions in cardiac muscle of pilot whales has also been reported to be age-related (Cowan, 1966), although such an association was not found in myocardium in this population. The overall prevalence of polysaccharide inclusions was highest in the current study of long-finned pilot whales (100%), compared with that reported in other cetacean species (22.6%) or short finned pilot whales (16.6%, 2/12 animals examined) (Sierra *et al*, 2012; Sierra *et al*, 2017). Cowan (1966) observed a prevalence (60%) of basophilic degeneration in long-finned pilot whales, which is closer to that in the present study. All of the animals in this study originated from the same pod, and so were highly likely to have been genetically related. Thus, it is unclear to what extent polysaccharide accumulation in long-finned pilot whales is a species-related phenomenon or whether there could have also been a familial component in this pod.

The most likely cause of stranding in this pod was an underwater explosion and the causes of death were attributable to the effects of live-stranding (Brownlow *et al*, 2015). Therefore, the physiological or pathophysiological origin and clinical significance of these inclusions remain elusive. The relative lack of associated histopathological features contrasts with the findings of acute necrosis and atrophy by Sierra *et al* (2012) despite chronic

myopathic and inflammatory changes being identified. As muscle weakness and dysfunction are a hallmark of polyglucosan body myopathies, it is possible that these inclusions could contribute to cetacean strandings but, in this species, are more likely to represent an incidental degenerative, age-related change unrelated to muscle dysfunction.

Screening future cases of stranded and non-stranded cetaceans for this lesion, including other populations of long-finned pilot whales unrelated to those examined here, may help determine the significance of this finding. Additionally, comparing long and deep-diving with short and non-deep diving cetacean species, may determine if longer episodes of hypoxia could contribute to this condition.

Acknowledgments

We thank Clare Underwood (MRI) and Valerie Forbes (MRI) for expert histological preparations, and Barry McGovern, Paul Jepson, Rob Deaville and Matt Perkins for collection of the tissue samples. This work was funded by the Scottish Government, the Moredun Research Institute, the Royal Zoological Society of Scotland and Marine Scotland.

Figure Legends

Fig. 1. Long-finned pilot whale. Intracytoplasmic inclusions comprising pale amphophilic to basophilic material in (a) skeletal and (b) cardiac myocytes. HE. Bar, 50 µm.

Fig. 2. Long-finned pilot whale, skeletal muscle. Periodic Acid-Schiff-positive, diastase-resistant inclusions, consistent with complex polysaccharide, at periphery of a skeletal myocyte. PAS-D. Bar, 100 µm.

Fig. 3. Long-finned pilot whale, skeletal muscle. (a) Intramyocytic inclusions stain black, consistent with carbohydrate. Grocott–Gomori's methenamine silver. Bar, 100 µm. (b) Inclusions are metachromatic indicating presence of acidic residues. Toluidine blue. Bar, 100 µm.

Fig. 4. Long-finned pilot whale, skeletal muscle. Mixed inflammatory response including macrophages and a few lymphocytes and neutrophils associated with inclusion-containing myocytes. (a) HE. Bar, 50 µm. (b) PAS-D. Bar, 50 µm.

Fig. 5a. Long-finned pilot whale, skeletal muscle. Non-membrane bound inclusion material (arrows) displaces myofibrils (M). Z-lines (Z). TEM. Bar, 2 µm.

Fig. 5b. Long-finned pilot whale, skeletal muscle. Higher magnification of short, loosely packed, randomly oriented and tangled filaments in inclusion. TEM. Bar, 1 µm.

Fig. 6a. Long-finned pilot whale, cardiac muscle. Distinct, non-membrane bound, intramyocytic inclusion mass (arrows) with central electron-dense core (C). Normal

295 myofibrils (M) and sarcomeric bands at periphery of cardiomyocyte. Erythrocyte (E).

296 Basement lamina (BM). TEM. Bar, 2 µm.

297

298 Fig. 6b. Long-finned pilot whale, cardiac muscle. Variegated, aggregated short fibrils form an

299 electron-dense core in which individual fibrils are not easily discernible. TEM. Bar, 0.2 µm.

References

Bancroft JD, Cook HC (1994) *Manual of histological techniques and their diagnostic applications,* Churchill Livingstone, Longman Group, United Kingdom.

Brownlow A, Baily J, Dagleish M, Deaville R, Foster G, *et al* (2015) Investigation into the long-finned pilot whale mass stranding event, Kyle of Durness, 22nd July 2011. SRUC Wildlife Unit, Inverness, UK, pp 60.

Cavanaugh JB (1999) Corpora–amylacea and the family of polyglucosan diseases. *Brain Research Reviews,* **29**, 265–295.

Cheville NF (2009) Polyglucosan body diseases. In: *Ultrastructural Pathology: the Comparative Cellular Basis of Disease,* 2nd Ed, p 868.

Cowan DF (1966) Pathology of the pilot whale *Globicephala melaena,* a comparative survey. *Archives of Pathology*, **82**, 178–189.

Ellis EA (2007) Post–staining grids for transmission electron microscopy: conventional and alternative protocols. In: *Electron Microscopy: Methods and Protocols.* 2nd J Kuo, Ed, Humana Press, Totowa, New Jersey, pp 99–102.

Hedberg–Oldfors C, Oldfors A (2015) Polyglucosan storage myopathies. *Molecular Aspects of Medicine,* **46**, 85–100.

Kuiken T, Baker J R (1991) Guidelines for the post-mortem examination of cetaceans. Zoological Society of London, London.

Larcher T, Herszberg B, Molon-Noblot S, Guigand L, Chaffaux S *et al* (2008) Polysaccharide storage myopathy in cob Normand draft horses. *Veterinary Pathology*, **45**, 154–158.

Luque PL, Learmonth JA, Santos MB, Ieno E, Pierce GJ (2009) Comparison of two histological techniques for age de termination in small cetaceans. *Marine Mammal Science,* **25,** 902−919.

McCue ME, Armién AG, Lucio M, Mickelson JR, Valberg SJ (2009) Comparative skeletal muscle histopathologic and ultrastructural features in two forms of polysaccharide storage myopathy in horses. *Veterinary Pathology*, **46**, 1281–1291.

McCue ME, Valberg SJ, Miller MB, Wade C, DiMauro S *et al* (2008) Glycogen synthase (GS1) mutation causes a novel skeletal muscle glycogenosis. *Genomics*, **91**, 458–466.

Naylor RJ, Livesey L, Schumacher J, Henke N, Massey C *et al* (2012) Allele copy number and underlying pathology are associated with subclinical severity in equine type 1 polysaccharide storage myopathy (PSSM1). *PLoS ONE,* **7**, e42317.

Reeves RR, Stewart BS, Clapham PJ, Powell JA (2002) Long-finned pilot whales. In: *Sea Mammals of the World*, A&C Black, London, pp 440–443.

Scotti TM (1962) Basophilic degeneration of the myocardium in a whale and a horse. *American Journal of Clinical Pathology*, **38**, 530–532.

Scottish Marine Animal Stranding Scheme (2020). https://www.strandings.org/cgi–bin/smass/map.pl. Accessed July 2020.

Sierra E, Fernández A, Espinosa de los Monteros A, Jaber JR, Andrada M *et al* (2012) Complex polysaccharide inclusions in the skeletal muscle of stranded cetaceans. *The Veterinary Journal*, **193**, 152–156.

Sierra E, Espinosa de Los Monteros A, Fernández A, Díaz-Delgado J, Suárez-Santana C *et al* (2017) Muscle pathology in free–ranging stranded cetaceans. *Veterinary Pathology*, **54**, 298–311.

Valberg SJ, McCue ME, Mickelson JR (2011) The interplay of genetics, exercise, and nutrition in polysaccharide storage myopathy. *Journal of Equine Veterinary Science*, **31**, 205–210.

Valentine BA, Credille KM, Lavoie JP, Fatone S, Guard C *et al* (1997) Severe polysaccharide storage myopathy in in Belgian and Percheron draught horses. *Equine Veterinary Journal*, **29**, 220–225.

Valentine BA, Cooper BJ (2006) Development of polyglucosan inclusions in skeletal muscle. *Neuromuscular Disorders*, **16**, 603–607.

374 Valentine BA, Flint TH, Fischer KA (2006) Ubiquitin expression in muscle from horses with
375 polysaccharide storage myopathy. *Veterinary Pathology*, **43,** 270–275.

Figure 1a

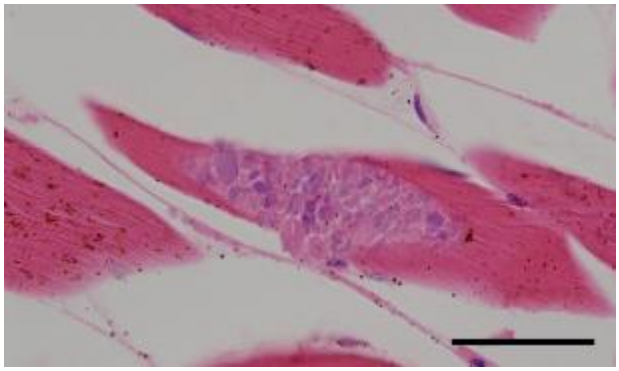

1b

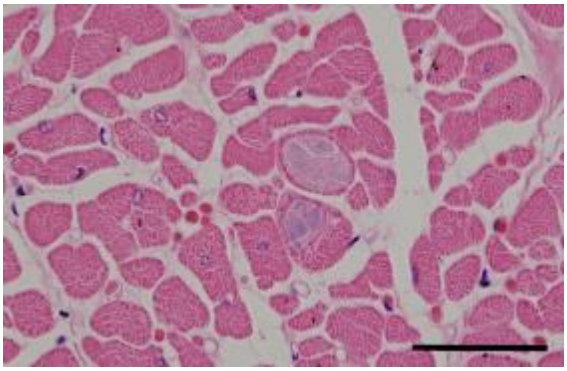

2

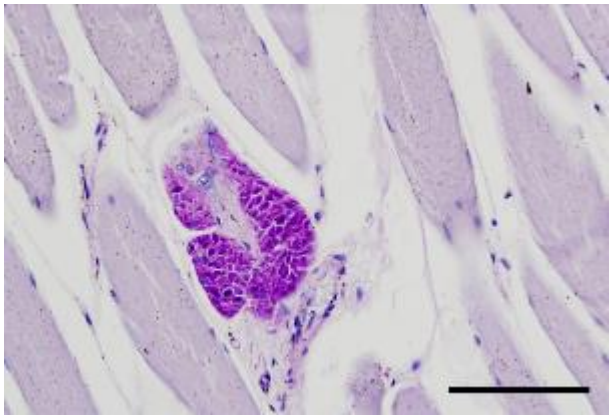

3a

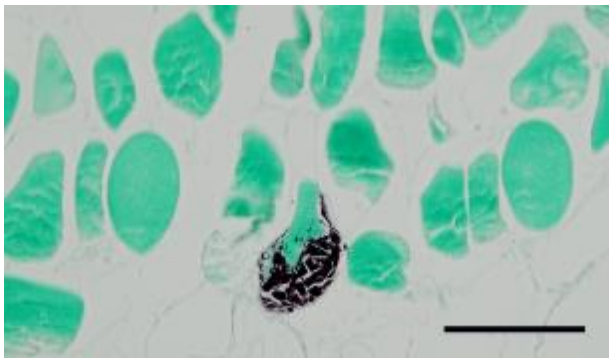

3b

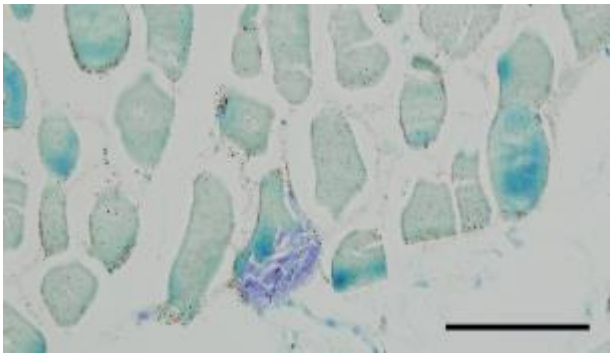

4a

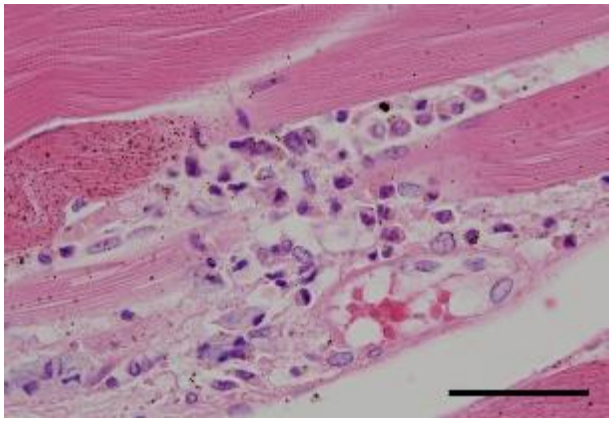

4b

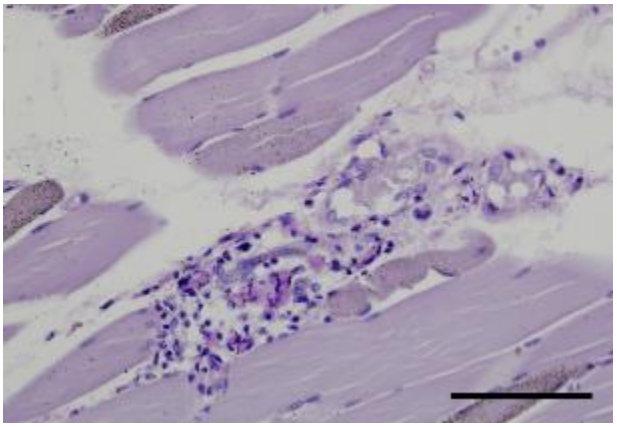

5a

Figure 5a.tif

5b

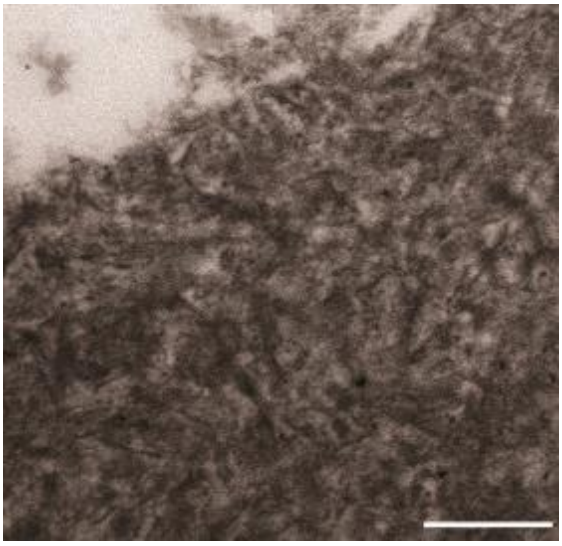

6a

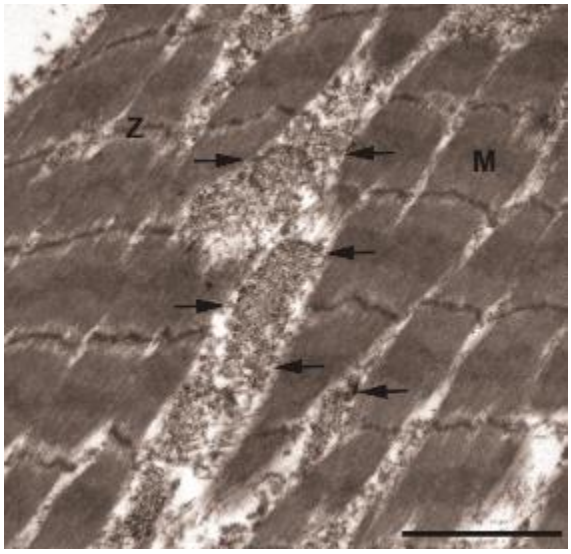

6b

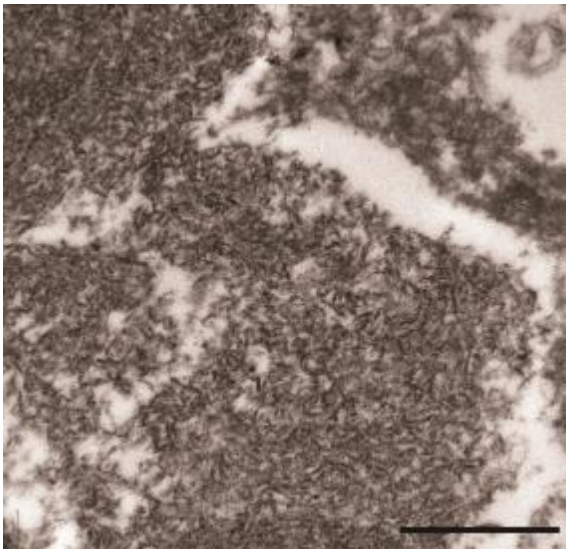

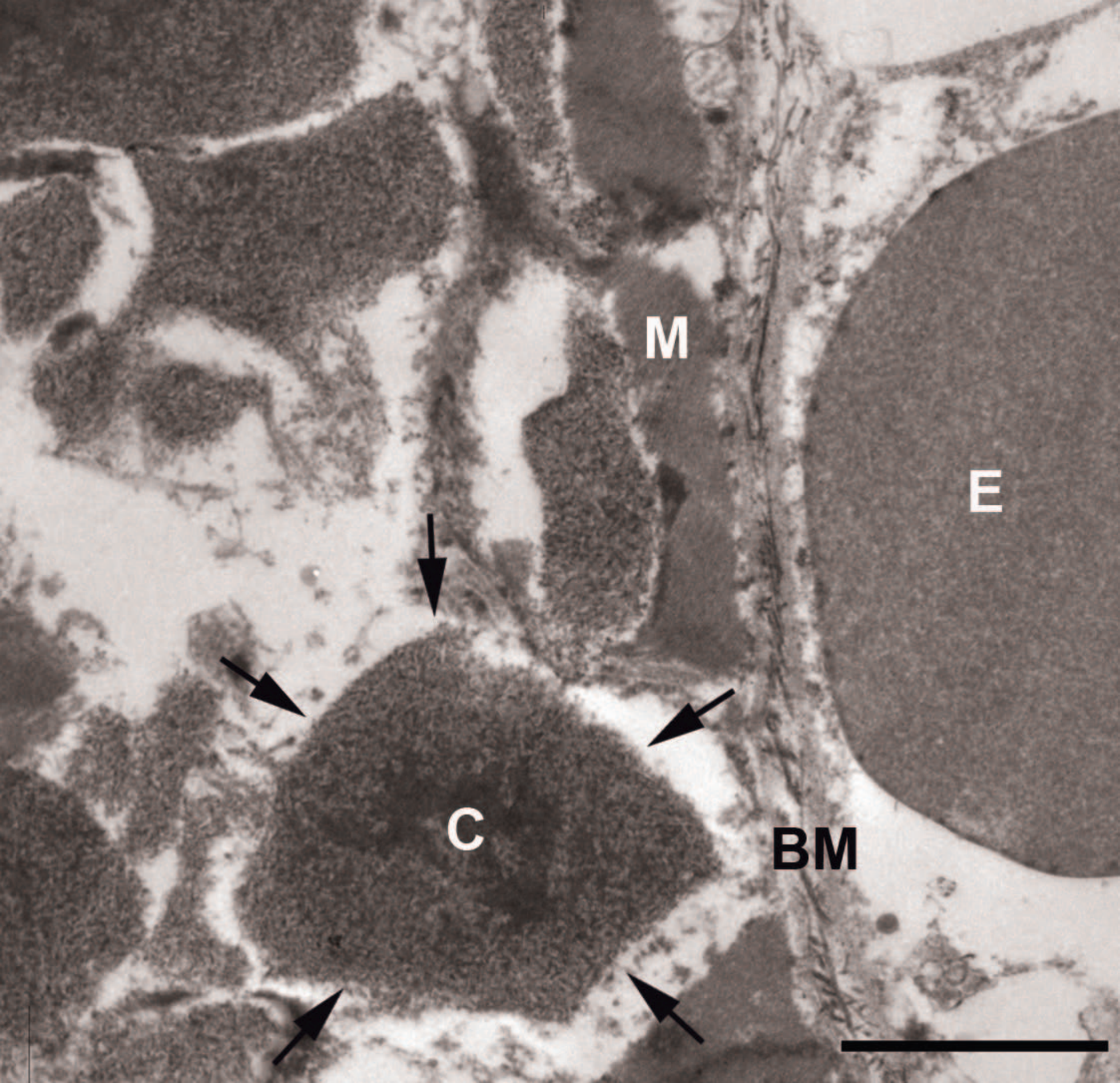
M
E
C
BM